Thermodynamic examination of quaternary compounds in the Ag–Fe–(Ge, Sn)–Se systems by the solid-state EMF method

Moroz, Mykola; Tesfaye, Fiseha; Demchenko, Pavlo; Prokhorenko, Myroslava; Rudyk, Bohdan; Soliak, Lyudmyla; Lindberg, Daniel; Reshetnyak, Oleksandr; Hupa, Leena

Published in:
Materials Processing Fundamentals 2021

DOI:
10.1007/978-3-030-65253-1_24

Published: 04/02/2021

Document Version
Accepted author manuscript

Document License
Publisher rights policy

§

Thermodynamic Examination of Quaternary Compounds in the Ag–Fe–(Ge, Sn)–Se Systems by the Solid-State EMF Method

Mykola Moroz,✉ Fiseha Tesfaye, Pavlo Demchenko, Myroslava Prokhorenko, Bohdan Rudyk, Lyudmyla Soliak, Daniel Lindberg, Oleksandr Reshetnyak, Leena Hupa

Abstract

The equilibrium phase space of the Ag–Fe–X–Se (X: Ge, Sn) systems in the parts Ag_8XSe_6–XSe–$FeSe_2$–$AgFeSe_2$–Ag_8XSe_6 consists of four quaternary-phase regions formed with the participation of low-temperature modifications of the $Ag_2FeGeSe_4$ and $Ag_2FeSnSe_4$ compounds. The kinetic barriers of the formation of equilibrium four-phase regions that are observed under conditions of vacuum ampoule synthesis below 600 K were overcome by synthesis of phases at the positive electrodes of electrochemical cells (ECCs): (−)C | Ag | SE | R (Ag^+) | PE | C(+), where C is graphite, Ag is left (negative) electrode, SE is the solid-state electrolyte, PE is the right (positive) electrode, and R (Ag^+) is the region of Ag^+ diffusion into PE. Silver cations Ag^+ that shifted from the left to the right electrode of ECCs acted as the seed centers of an equilibrium set of phases. Based on the temperature dependences of the EMF of the cells in the temperature range 430–485 K, the standard thermodynamic functions of the $Ag_2FeGeSe_4$ and $Ag_2FeSnSe_4$ compounds were calculated for the first time. The observed experimental results and thermodynamic calculations are in good agreement.

Keywords Silver-based phases, Magnetic semiconductors, Phase equilibria, Standard thermodynamic properties, EMF method, Gibbs energy

1. Introduction

Quaternary chalcogenides with a general formula is A_2BYZ_4 (A: Cu, Ag; B: Zn, Cd, Hg, Mn, Fe, Co, Ni; Y: Si, Ge, Sn, Pb; Z: S, Se, Te) are representative of a group of compounds, that mostly crystallize in the tetragonal stannite or in the orthorhombic wurtzite-stannite structures [1–9]. These compounds can be defined as tetrahedral chalcogenides, because all of the anions or cations are fourfold-surrounded by their neighboring [10]. Many publications in recent decades are focused on study of these tetrahedral chalcogenides due to their potential application as economic functional materials in the solar cells, thermoelectric, photocatalytic, and photovoltaic devices [6,10–12]. Moreover, tetrahedral chalcogenides with transition metal ions such as Ni^{2+}, Fe^{2+}, Co^{2+}, and Mn^{2+} exhibit large magneto-optical effects. According to some researchers [10,13,14], the $Cu_2FeGeSe_4$ and $Cu_2FeSnSe_4$ compounds are antiferromagnetic with a Neel temperature at T_N=20 K and T_N=19 K, respectively. The $Cu_2FeGeTe_4$ is ferromagnetic with T_N~160.1 K [13]. The Ag-containing magnetic tetrahedral chalcogenides have been rarely discussed until now due to difficult condition of synthesis of a homogeneous material and narrow

M. Moroz (✉)
Department of Chemistry and Physics, National University of Water and Environmental Engineering, Rivne, 33028, Ukraine
Department of Physical and Colloid Chemistry, Ivan Franko National University of Lviv, Lviv, 79005, Ukraine
e-mail: m.v.moroz@nuwm.edu.ua

F. Tesfaye, L. Hupa
Johan Gadolin Process Chemistry Centre, Åbo Akademi University, Turku, 20500, Finland

P. Demchenko
Department of Inorganic Chemistry, Ivan Franko National University of Lviv, Lviv,79005, Ukraine

M. Prokhorenko
Department of Cartography and Geospatial Modeling, Lviv Polytechnic National University, Lviv,79013, Ukraine

B. Rudyk, L. Soliak
Department of Chemistry and Physics, National University of Water and Environmental Engineering, Rivne, 33028, Ukraine

D. Lindberg
Department of Chemical and Metallurgical Engineering, Aalto University, Kemistintie 1, Espoo, 02150, Finland

O. Reshetnyak
Department of Physical and Colloid Chemistry, Ivan Franko National University of Lviv, Lviv, 79005, Ukraine

§

thermal stability range [2,11,15]. Nevertheless, physical properties of the $Ag_2FeGeSe_4$ compound have been investigated by several authors [3,16,17]. Wooley et al. [3] established the high field magnetic properties of the $Ag_2FeGeSe_4$ in the range of T=(2–300) K. It was found that at T_N=240 K quaternary compound shows mainly antiferromagnetic behavior, with a weak superimposed ferromagnetic component down to T=60 K. Below T=60 K the ferromagnetic component becomes much bigger. The magnetic spin-flop, critical-fields, and magnetic saturation in the $Ag_2FeGeSe_4$ were reported in [16,17]. Information on the $Ag_2FeSnSe_4$ compound is limited by data on the temperature of formation during cooling of the melt, the crystal structure of its high-temperature modification [2]. No information on the thermodynamic properties of quaternary compounds of the Ag–Fe–X–Se (X: Ge, Sn) system was found in the open literature.

The purpose of this work was to demonstrate the capabilities of solid-state synthesis from elements of equilibrium set of compounds in the Ag–Fe–X–Se systems in the range of T=(400–500) K, where the energy of the thermal motion of atoms is insufficient for the formation of the nucleation centers of phases; and to determine thermodynamic properties of the quaternary compounds in the investigated systems by applying the electromotive force (EMF) method.

2. Experimental Section

2.1. Synthesis and analysis

The starting materials for synthesis were high-purity elements (99.99 wt% Ag, 99.9 wt% Fe, 99.999 wt% Ge, 99.999 wt% Sn, 99.99 wt% S, and 99.99 wt% Se). The samples of the formula compositions '$Ag_2FeGeSe_4$' and '$Ag_2FeSnSe_4$' for X-ray diffraction (XRD) were synthesized by two methods:

1) solid-state synthesis of the calculated mixture of elements in evacuated ($p \sim 10^{-2}$ Pa) quartz ampoules at T=630 K during 5 days. The samples were cooled to room temperature at the rate of 2 K·min^{-1} and ground to particle size of ~5.0 μm. Vacuum homogenization of the fine phase mixture was held at T=580 K for 5 days.

2) vacuum melting of the calculated mixture of elements at T=1100 K followed by vacuum annealing of the finely disperse mixture at T=580 K for 5 days.

The synthesis of an equilibrium set of phases for the study of the thermodynamic properties of low-temperature modifications of the $Ag_2FeGeSe_4$ and $Ag_2FeSnSe_4$ compounds was performed in the positive electrodes (PE) of electrochemical cells (ECCs).

XRD patterns were collected on an STOE STADI P diffractometer equipped with a linear position-sensitive detector PSD, in a modified Guinier geometry (transmission mode, Cu$K\alpha_1$ radiation, a bent Ge (111) monochromator, $2\theta/\omega$ scan mode). Preliminary data processing and X-ray phase analyses were performed using STOE WinXPOW 3.03 [18] and Powder Cell 2.4 PC programs [19], using data on crystal structures for the phases taken from the database [20].

The Ag_2GeS_3 glass [21–23] was obtained by melt quenching of the corresponding elements from T=1200 K in ice water.

2.2. Electromotive Force Measurements

For the EMF measurements, the following ECCs were assembled:

$$(-)\text{C} \mid \text{Ag} \mid \text{SE} \mid \text{R}\,(\text{Ag}^+) \mid \text{PE} \mid \text{C}(+), \qquad \text{(A)}$$

where C is graphite, Ag is left (negative) electrode, SE is the solid-state electrolyte, PE is the right (positive) electrode, R (Ag^+) is the region of Ag^+ penetration into PE. Pure silver powder was used as a left electrode. Ag_2GeS_3 glass was used as SE with purely Ag^+ ionic conductivity [21,24].

PE at the stage of the cell preparation is a well-mixed composition of finely ground mixtures of elements Ag, Fe, Ge (Sn), and Se, with particle size ~5 μm. The ratios of the elements were determined from the equations of the potential-forming reactions in respective phase fields. ECC components in powder form were pressed at 10^8 Pa through a 2 mm diameter hole arranged in the fluoroplast matrix up to density $\rho = (0.93 \pm 0.02)\cdot\rho_0$, where ρ_0 is the experimentally determined density of cast samples [25].

EMF measurements were performed in a horizontal resistance furnace, similar to that described in [26]. As protective atmosphere, we used a continuously flowing highly purified (0.9999 volume fraction) Ar(g) at $P = 1.2\cdot10^5$ Pa, with a flow rate of $2\cdot10^{-3}$ m^3·h^{-1} from the left to right electrode of the ECCs. The temperature was maintained with an accuracy of ±0.5 K. The EMF (E) of the cells were measured by high-resistance (input impedance of $>10^{12}$ Ω) universal U7-9 digital voltmeter and MTech PGP-550M device. The heating and cooling rates were 2 K·min^{-1}. The equilibrium in ECCs at each temperature was achieved within ≤1 h. The criterion of achieving the equilibrium state in the PE was the reproducibility of the E versus T dependences in the heating-cooling cycles. The scheme of ECCs and procedure of the EMF measurements have been described in our previous works [27–29].

3. Results and Discussion

§

The $Ag_2FeGeSe_4$ and $Ag_2FeSnSe_4$ compounds have not been obtained by vacuum ampoule melting and annealing of the components described in Sec. 2. The diffraction patterns of both samples are shown in Fig. 1 and 2. The presence of the phases (Ag_8GeSe_6, Fe_2GeSe_4, and $GeSe_2$) in the sample '$Ag_2FeGeSe_4$' and (Ag_8SnSe_6, Ag_2Se, $AgSnSe_2$, and Fe_3Se_4) in the sample '$Ag_2FeSnSe_4$' has been established by XRD method. Increasing the annealing time to 20 days in the range of T=(450–600) K does not change the diffraction pattern of the samples. Thus, no signs of the formation of the $Ag_2FeGeSe_4$ and $Ag_2FeSnSe_4$ compounds were detected under the described conditions of vacuum ampoule synthesis and annealing of the samples.

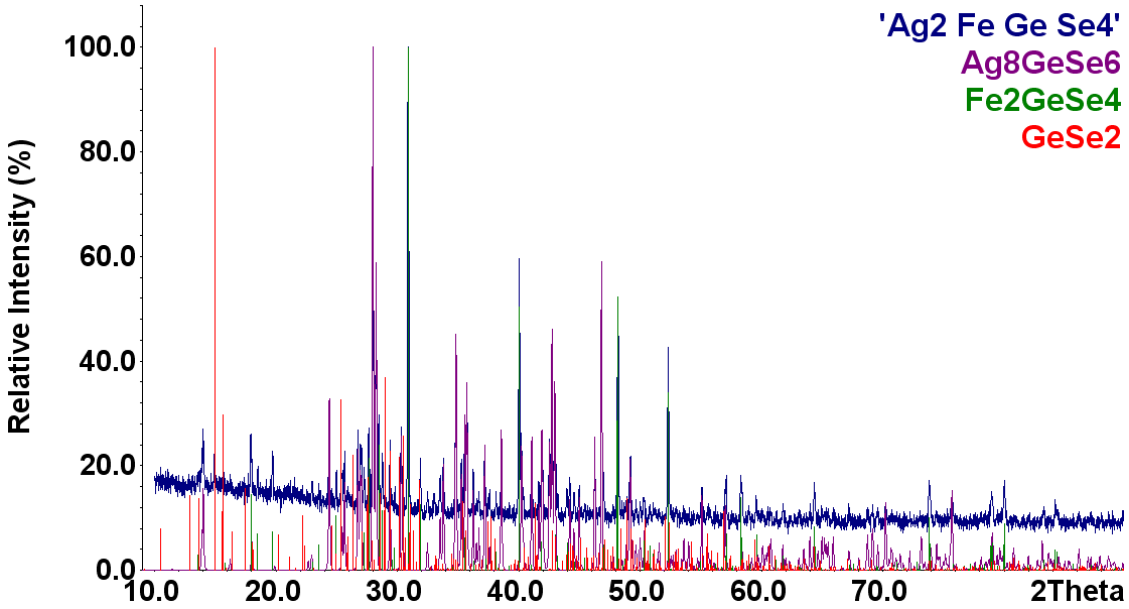

Fig. 1 Comparison of the experimental XRD pattern of the sample '$Ag_2FeGeSe_4$' with those theoretical patterns of the compounds

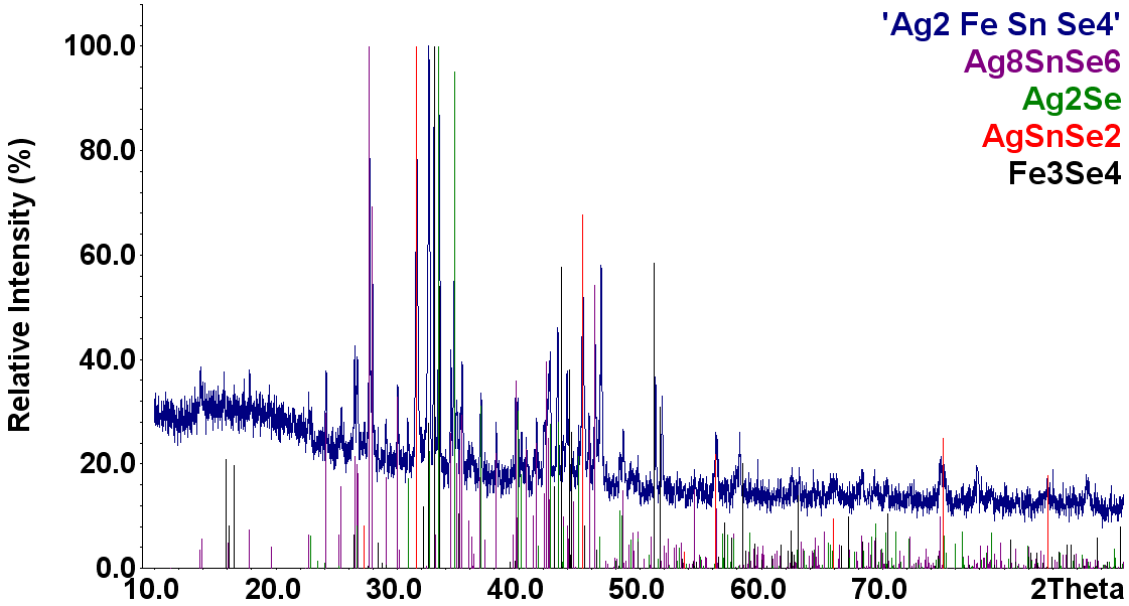

Fig. 2 Comparison of the experimental XRD pattern of the sample '$Ag_2FeSnSe_4$' with those theoretical patterns of the compounds

Our work on synthesis and study thermodynamic parameters of low-temperature modifications of the $Ag_2FeGeSe_4$ and $Ag_2FeSnSe_4$ compounds, as in case of $Ag_2FePbSe_4$ [15], are based on the following:

a) identified by XRD method the phase compositions of the '$Ag_2FeGeSe_4$' and '$Ag_2FeSnSe_4$' samples is considered metastable for kinetic reasons at T<600 K;

b) the validity of the proposed division of the equilibrium concentration space of the Ag–Fe–X–Se systems in the parts Ag_8XSe_6–XSe–$FeSe_2$–$AgFeSe_2$–Ag_8XSe_6 into separate four-phase regions;

c) possibility of the solid-state synthesis of equilibrium set of phases in the PE of ECCs.

§

In type (A) ECC, self-motion of Ag^+ cations from the left to the right electrode takes place due to differences in the chemical potentials of silver in these areas [30]. The consequence of such a movement is the appearance of a potential difference at the electrodes of the ECC. Solid-state synthesis of the equilibrium set of phases was performed in the PE of ECC at the penetration depth of Ag^+ ions, i.e. the R (Ag^+) region. It was found that EMF values in the newly assembled ECCs change over time at T=const. This is as a result of the diffusion processes and intermediate reactions in the metastable set of phases of the R(Ag^+) region. The positive charge localized in the R(Ag^+) region reduces the Coulomb repulsive forces between the components of the PE to the values of ≤0. This is a condition for non-activation synthesis of the equilibrium set of phases. Ag^+ cations are not a phase, do not chemically interact with a metastable set of elements, but act as a catalyst for non-activation synthesis. In the R(Ag^+) region, the spatial grouping of individual phases of the equilibrium set is carried out by diffusion of atoms and is a function of temperature. The process of forming an equilibrium set of phases ends in ≤5 hrs for the particle size of the heterogeneous phase mixture ~5 μm at T=500 K. It was not possible to isolate the equilibrium mixture of phases for XRD due to its negligible amount, similarly to the case in [31]. An example of solid-state synthesis of the rather simple phase AgTe in the ECC is presented in [32].

The phase equilibria of the Ag–Fe–X–Se systems in the parts Ag_8XSe_6–XSe–$FeSe_2$–$AgFeSe_2$–Ag_8XSe_6 are shown in Fig. 3.

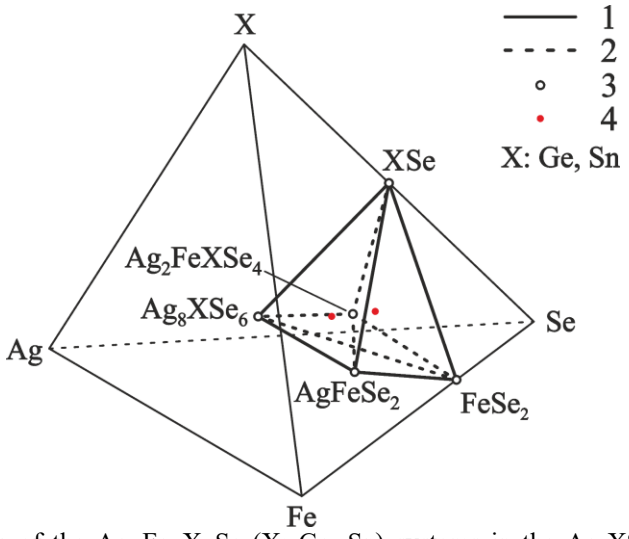

Fig. 3 The phase equilibria of the Ag–Fe–X–Se (X: Ge, Sn) systems in the Ag_8XSe_6–XSe–$FeSe_2$–$AgFeSe_2$–Ag_8XSe_6 parts, below 500 K. The solid and dashed tie lines (1 and 2) indicate two-phase equilibria, the open circle (3) indicate compounds, and the red closed circle (4) indicate compositions of positive electrodes of ECCs

Division of the concentration space into separate regions was performed according to the results of Refs. [15,33–37] and the present study by the EMF method. The presence of four 4-phase regions has been established: Ag_8XSe_6–Ag_2FeXSe_4–XSe–$AgFeSe_2$ **(I)**, Ag_8XSe_6–Ag_2FeXSe_4–XSe–$FeSe_2$ **(II)**, Ag_8XSe_6–Ag_2FeXSe_4–$AgFeSe_2$–$FeSe_2$, and XSe–Ag_2FeXSe_4–$AgFeSe_2$–$FeSe_2$. The correctness of the suggested limits of four-phase regions is confirmed by the following calculations of thermodynamic quantities for the $Ag_2FeGeSe_4$ and $Ag_2FeSnSe_4$ compounds.

The position of the phase regions **(I)** and **(II)** relative to Ag was used to write the equations of the overall potential-forming reactions of decomposition and synthesis of the quaternary compounds:

$$3Ag + 5Ag_2FeGeSe_4 = Ag_8GeSe_6 + 5AgFeSe_2 + 4GeSe, \quad (R1)$$

$$2Ag + Ag_8GeSe_6 + 4GeSe + 5FeSe_2 = 5Ag_2FeGeSe_4, \quad (R2)$$

$$3Ag + 5Ag_2FeSnSe_4 = Ag_8SnSe_6 + 5AgFeSe_2 + 4SnSe, \quad (R3)$$

$$2Ag + Ag_8SnSe_6 + 4SnSe + 5FeSe_2 = 5Ag_2FeSnSe_4. \quad (R4)$$

In accordance with reactions (R1)–(R4), the compositions of the positive electrodes in the phase regions **(I)** and **(II)** were determined by element ratios Ag: Fe: Ge: Se of 23: 10: 10: 20 and 9: 5: 5: 20 for the Ag–Fe–Ge–Se system; with the element ratios Ag: Fe: Sn: Se of 23: 10: 10: 20 and 9: 5: 5: 20, for the Ag–Fe–Sn–Se system, respectively.

The measured EMF values of the ECCs at various temperatures in the range of T=(430–485) K are shown in Fig. 4 and can be expressed by Eqs. (1)–(4):

$$E_{(R1)}/\text{mV} = (110.15\pm0.87) + (380.26\pm1.90)\cdot10^{-3}T/\text{K}, R^2=0.99973, \quad (1)$$

$$E_{(R2)}/\text{mV} = (160.58\pm0.79) + (350.15\pm1.72)\cdot10^{-3}T/\text{K}, R^2=0.99973, \quad (2)$$

§

$$E_{(R3)}/\text{mV} = (207.50\pm1.22) + (225.17\pm2.67)\cdot10^{-3}T/\text{K},\ R^2=0.99846, \quad (3)$$

$$E_{(R4)}/\text{mV} = (225.07\pm0.60) + (262.78\pm1.32)\cdot10^{-3}T/\text{K},\ R^2=0.99972, \quad (4)$$

where R^2 is the coefficient of determination. The upper and lower limits of the temperature range of the measurements were determined by the linear part of the E versus T dependences that were reproducible in the heating-cooling cycles.

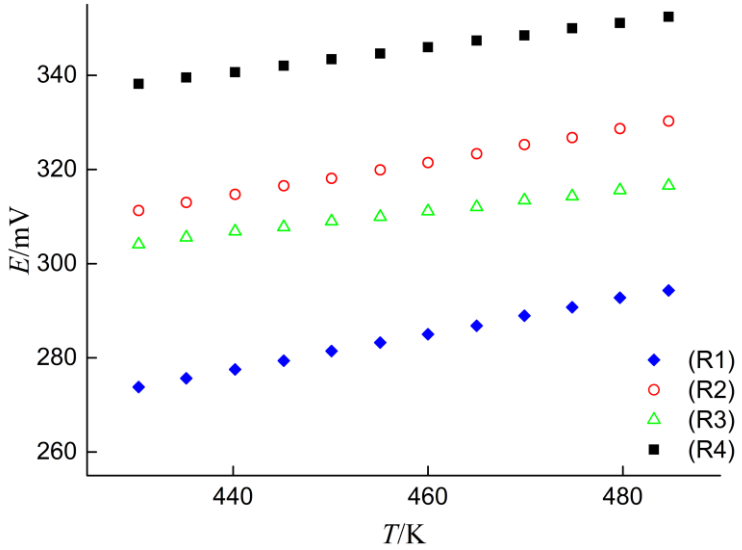

Fig. 4 EMF values of the ECCs as a function of cell temperature

The Gibbs energies, entropies, and enthalpies of the reactions (R1)–(R4) can be calculated by combining the measured EMF values of each ECCs and the thermodynamic Eqs. (5)–(7):

$$\Delta_r G = -n \cdot \text{F} \cdot E, \quad (5)$$

$$\Delta_r H = -n \cdot \text{F} \cdot [E - (dE/dT) \cdot T], \quad (6)$$

$$\Delta_r S = n \cdot \text{F} \cdot (dE/dT), \quad (7)$$

where n is the number of electrons involved in the reactions (R1)–(R4), F = 96485.33289 C·mol^{-1} is Faraday constant, and E in V is the EMF of the ECCs.

Standard thermodynamic quantities of the reactions (R1)–(R4) at T=298 K were calculated using Eqs. (5)–(7) in the approximation $\left(\frac{\partial \Delta_r H}{\partial T}\right)_p = 0$ and $\left(\frac{\partial \Delta_r S}{\partial T}\right)_p = 0$ [32,38]. The results of the calculations are presented in Table 1.

Table 1 Standard thermodynamic quantities of the reactions (R1)–(R4) in the ECCs

Reaction	$-\Delta_r G^\circ$	$-\Delta_r H^\circ$	$\Delta_r S^\circ$
	kJ·mol^{-1}		J·(mol·K)$^{-1}$
(R1)	64.70 ± 0.86	31.88 ± 0.25	110.07 ± 0.55
(R2)	51.13 ± 0.52	30.99 ± 0.15	67.57 ± 0.33
(R3)	79.49 ± 1.44	60.06 ± 0.35	65.18 ± 0.77
(R4)	58.55 ± 0.47	43.43 ± 0.12	50.71 ± 0.25

In the phase region **(I)** standard Gibbs energy and entropy of reaction (R1) are related to the Gibbs energy of formation and entropy of compounds and pure elements the following equations:

$$\Delta_{r(R1)}G^\circ = \Delta_f G^\circ_{Ag_8GeSe_6} + 5\Delta_f G^\circ_{AgFeSe_2} + 4\Delta_f G^\circ_{GeSe} - 5\Delta_f G^\circ_{Ag_2FeGeSe_4}, \quad (8)$$

$$\Delta_{r(R1)}S^\circ = S^\circ_{Ag_8GeSe_6} + 5S^\circ_{AgFeSe_2} + 4S^\circ_{GeSe} - 3S^\circ_{Ag} - 5\Delta_f G^\circ_{Ag_2FeGeSe_4}. \quad (9)$$

It follows from Eqs. (8) and (9) that:

$$\Delta_f G^\circ_{Ag_2FeGeSe_4} = 0.2\left(\Delta_f G^\circ_{Ag_8GeSe_6} + 5\Delta_f G^\circ_{AgFeSe_2} + 4\Delta_f G^\circ_{GeSe} - \Delta_{r(R1)}G^\circ\right), \quad (10)$$

$$S^\circ_{Ag_2FeGeSe_4} = 0.2\left(S^\circ_{Ag_8GeSe_6} + 5S^\circ_{AgFeSe_2} + 4S^\circ_{GeSe} - 3S^\circ_{Ag} - \Delta_{r(R1)}S^\circ\right). \quad (11)$$

The entropy of formations of the $Ag_2FeGeSe_4$ compound can be calculated as:

$$\Delta_f S^\circ_{Ag_2FeGeSe_4} = S^\circ_{Ag_2FeGeSe_4} - 2S^\circ_{Ag} - S^\circ_{Fe} - S^\circ_{Ge} - 4S^\circ_{Se}. \quad (12)$$

§

The corresponding reactions to determine $\Delta_f G^\circ$, S°, and $\Delta_f S^\circ$ for the $Ag_2FeGeSe_4$ in the phase region **(II)** and for the $Ag_2FeSnSe_4$ in the phase regions **(I)** and **(II)** can be written similar to Eqs. (10)–(12) with their appropriate stochiometric numbers.

Combining Eqs. (5)–(7) and (10)–(12), using thermodynamic data of the pure elements [39], and compounds GeSe [39], SnSe [39], $FeSe_2$ [40], $AgFeSe_2$ [15], Ag_8GeSe_6 [30], Ag_8SnSe_6 [30], the standard Gibbs energy of formations of quaternary compounds of the Ag–Fe–X–Se systems in the phase regions **(I)** and **(II)** were calculated. A comparative summary of the calculated values together with the available literature data is presented in Table 2.

Table 2 Standard thermodynamic quantities of selected phases in the Ag–Fe–X–Se systems

Phases	$-\Delta_f G^\circ$	$-\Delta_f H^\circ$	S°	[Ref.]
	kJ·mol^{-1}		J·(mol·K)$^{-1}$	
Ag	0	0	42.677	[39]
Fe	0	0	27.280	[39]
Ge	0	0	31.087	[39]
Sn	0	0	51.195	[39]
Se	0	0	42.258	[39]
GeSe	70.496	69.036	78.241	[39]
SnSe	87.533	88.701	89.538	[39]
$FeSe_2$	101.3 ± 15.0	108.7 ± 15.0	86.8 ± 1.0	[40]
$AgFeSe_2$	125.9 ± 15.0	128.8 ± 15.0	144.7 ± 3.3	[15]
Ag_8GeSe_6	288.0 ± 2.3	255.0 ± 2.8	734.6 ± 30.4	[30]
Ag_8SnSe_6	350.3 ± 1.8	320.4 ± 8.1	746.4 ± 23.8	[30]
$Ag_2FeGeSe_4$[a]	227.0 ± 34.6	228.7 ± 27.5	307.0 ± 9.9	This work
$Ag_2FeGeSe_4$[b]	225.5 ± 36.3	221.1 ± 31.2	327.3 ± 6.5	This work
$Ag_2FeSnSe_4$[a]	250.1 ± 38.6	251.8 ± 30.9	327.0 ± 10.4	This work
$Ag_2FeSnSe_4$[b]	253.0 ± 40.9	252.4 ± 36.3	334.9 ± 6.0	This work

[a] phase region **(I)**
[b] phase region **(II)**

The temperature dependences of the Gibbs energies of formation of the quaternary compounds in the phase regions **(I)** and **(II)** are described as:

$$\Delta_f G_{Ag_2FeGeSe_4,(I)}/(\text{kJ·mol}^{-1}) = -(228.7 \pm 27.5) + (5.7 \pm 0.2) \cdot 10^{-3} T/\text{K}, \quad (13)$$

$$\Delta_f G_{Ag_2FeGeSe_4,(II)}/(\text{kJ·mol}^{-1}) = -(221.1 \pm 31.2) - (14.6 \pm 0.3) \cdot 10^{-3} T/\text{K}, \quad (14)$$

$$\Delta_f G_{Ag_2FeSnSe_4,(I)}/(\text{kJ·mol}^{-1}) = -(251.8 \pm 30.9) + (5.9 \pm 0.2) \cdot 10^{-3} T/\text{K}, \quad (15)$$

$$\Delta_f G_{Ag_2FeSnSe_4,(II)}/(\text{kJ·mol}^{-1}) = -(252.4 \pm 36.3) - (2.1 \pm 0.1) \cdot 10^{-3} T/\text{K}. \quad (16)$$

It follows from Eqs. (13)–(16) that the enthalpy and entropy values of the Gibbs energy of formation of the quaternary compounds differ in phase regions **(I)** and **(II)**, with entropy of the reaction differing not only in magnitude but also in sign. These differences are due to the different nature of the crystal lattice defects in the solid solutions of the compounds that is in equilibrium in these phase regions. At the same time, the convergence within the experiment error of the calculated $\Delta_f G^\circ$ values for the $Ag_2FeGeSe_2$ and $Ag_2FeSnSe_2$ compounds in the phase regions **(I)**, **(II)** (the relative differences are ~1%) serves as the validation to correctness:

a) phase composition and division of the equilibrium concentration space of the Ag–Fe–X–Se systems in the parts Ag_8XSe_6–XSe–$FeSe_2$–$AgFeSe_2$–Ag_8XSe_6;
b) calculated values of the thermodynamic quantities of the quaternary compounds;
c) reliability of the literature values of the thermodynamic properties of compounds GeSe, SnSe, $FeSe_2$, Ag_8GeSe_6, Ag_8SnSe_6, and $AgFeSe_2$; and
d) negligible homogeneity region of the $Ag_2FeGeSe_4$ and $Ag_2FeSnSe_4$ compounds.

4. Conclusions

Division of the equilibrium concentration space of the Ag–Fe–X–Se (X: Ge, Sn) systems in the parts Ag_8XSe_6–XSe–$FeSe_2$–$AgFeSe_2$–Ag_8XSe_6 into four quaternary-phase regions were established. The positions of the phase regions Ag_8XSe_6–Ag_2FeXSe_4–XSe–$AgFeSe_2$ and Ag_8XSe_6–Ag_2FeXSe_4–XSe–$FeSe_2$ versus the point of Ag were used to write the equations of overall potential-forming reactions. Solid-state synthesis of the equilibrium set of phases, including the quaternary compounds, was performed in the positive electrodes of electrochemical cells. Ag^+ cations that shifted from the left electrode are catalysts for the formation of nucleation centers of individual phases.

§

Linear dependences of the EMF versus T of the ECCs were used for calculations of the standard Gibbs energies, enthalpies, and entropies of formations of the quaternary compounds. Calculations were performed in two fundamentally different potential-forming processes: the decomposition and synthesis of the quaternary compounds. The agreement of the determined $\Delta_f G^\circ$ values in the two potential-forming processes confirm that: the division of the concentration space of the Ag–Fe–X–Se systems and the phase composition of the positive electrodes in the ECCs used to calculate the thermodynamic properties of the $Ag_2FeGeSe_4$ and $Ag_2FeSnSe_4$. Furthermore, the reproducibility of the determined $\Delta_f G^\circ$ confirms the accuracy of the literature Gibbs energy data for GeSe, SnSe, $FeSe_2$, Ag_8GeSe_6, Ag_8SnSe_6, and $AgFeSe_2$.

Acknowledgements

This work was partially supported by the Ministry of Education and Science of Ukraine (grant No. 0119U002208). This work was also financially supported by the Academy of Finland project "Thermodynamic investigation of complex inorganic material systems for improved renewable energy and metals production processes" (Decision number 311537), as part of the activities of the Johan Gadolin Process Chemistry Center at Åbo Akademi University.

Conflict of Interest

The authors declare that they have no conflict of interest.

References

1. Fries T, Shapira Y, Palacio F, Morón MC, McIntyre GJ, Kershaw R, Wold A, McNiff EJ (1997) Magnetic ordering of the antiferromagnet Cu_2MnSnS_4 from magnetization and neutron-scattering measurements. Phys Rev B 56:5424–5431

2. Quintero M, Barreto A, Grima P, Tovar R, Quintero E, Porras GS, Ruiz J, Woolley JC, Lamarche G, Lamarche A-M (1999) Crystallographic properties of I_2–Fe–IV–VI_4 magnetic semiconductor compounds. Mater Res Bull 34:2263–2270

3. Woolley JC, Lamarche G, Lamarche A-M, Rakoto H, Broto JM, Quintero M, Morocoima M, Quintero E, Gonzalez J, Tovar R, Cadenas R, Bocoranda P, Ruiz J (2003) High field magnetic properties of $Ag_2FeGeSe_4$ in the temperature range 2–300K. J Magn Magn Mater 257:87–94

4. Sachanyuk VP, Olekseyuk ID, Parasyuk OV (2006) X-ray powder diffraction study of the $Cu_2Cd_{1-x}Mn_xSnSe_4$ alloys. Phys Status Solidi (a) 203:459–465

5. Chen S, Walsh A, Luo Y, Yang J-H, Gong XG, Wei S-H (2010) Wurtzite-derived polytypes of kesterite and stannite quaternary chalcogenide semiconductors. Phys Rev B 82:195203(1–8)

6. Prabhakar RR, Zhenghua S, Xin Z, Baikie T, Woei LS, Shukla S, Batabyal SK, Gunawan O, Wong LH (2016) Photovoltaic effect in earth abundant solution processed Cu_2MnSnS_4 and $Cu_2MnSn(S,Se)_4$ thin films. Sol Energy Mater Sol Cells 157:867–873

7. Chen L, Deng H, Tao J, Cao H, Sun L, Yang P, Chu J (2016) Strategic improvement of Cu_2MnSnS_4 films by two distinct post-annealing processes for constructing thin film solar cells. Acta Mater 109:1–7

8. Rondiya S, Wadnerkar N, Jadhav Y, Jadkar S, Haram S, Kabir M (2017) Structural, electronic, and optical properties of Cu_2NiSnS_4: a combined experimental and theoretical study toward photovoltaic applications. Chem Mater 29:3133–3142

9. Heppke EM, Berendts S, Lerch M (2020) Crystal structure of mechanochemically synthesized Ag_2CdSnS_4. Z Naturforsch B 75:393–402

10. Chen M-M, Xue H-G, Guo S-P (2018) Multinary metal chalcogenides with tetrahedral structures for second-order nonlinear optical, photocatalytic, and photovoltaic applications. Coord Chem Rev 368:115–133

11. Heppke EM, Klenner S, Janka O, Pöttgen R, Lerch M (2020) Mechanochemical synthesis of $Cu_2MgSn_3S_8$ and $Ag_2MgSn_3S_8$. Z Anorg Allg Chem 646:5–9

12. Liu W, Hu J, Zhang S, Deng M, Han C-G, Liu Y (2017) New trends, strategies and opportunities in thermoelectric materials: a perspective. Mater Today Phys 1:50–60

13. Quintero E, Quintero M, Morocoima M, Bocaranda P (2007) Bound magnetic polarons in p-type $Cu_2Cd_{0.25}Fe_{0.75}GeSe_4$ and $Cu_2FeGeTe_4$. J Appl Phys 102:083905(1–5)

14. Quintero E, Quintero M, Moreno E, Lara L, Morocoima M, Pineda F, Grima P, Tovar R, Bocaranda P, Henao JA, Macías MA (2010) Magnetic properties for the $Cu_2MnSnSe_4$ and $Cu_2FeSnSe_4$ compounds. J Phys Chem Solids 71:993–998

15. Moroz M, Tesfaye F, Demchenko P, Prokhorenko M, Kogut Y, Pereviznyk O, Prokhorenko S, Reshetnyak O (2020) Solid-state electrochemical synthesis and thermodynamic properties of selected compounds in the Ag–Fe–Pb–Se system. Solid State Sci 107:106344(1–9)

§

16. Quintero M, Cadenas R, Tovar R, Quintero E, Gonzalez J, Ruiz J, Woolley JC, Lamarche G, Lamarche A-M, Broto JM, Rakoto H, Barbaste R (2001) Magnetic spin-flop and magnetic saturation in $Ag_2FeGeSe_4$, $Ag_2FeSiSe_4$ and $Cu_2MnGeSe_4$ semiconductor compounds. Physica B: Condensed Matter 294–295:471–474

17. Marquina J, Sierralta N, Quintero M, Rincon C, Morocoima M, Quintero E (2017) Study of the critical-fields and the thermal broadening in polycrystalline $Ag_2FeGeSe_4$ semiconducting compound. Revista Mexicana de Fisica 63:456–460

18. Diffractom. Stoe WinXPOW, Version 3.03 (2010) Stoe Cie GmbH Darmstadt

19. Kraus W, Nolze G (1996) Powder Cell – a program for the representation and manipulation of crystal structures and calculation of the resulting X-ray powder patterns. J Appl Crystallogr 29:301–303

20. Villars P, Cenzual K (2014) Pearson's crystal data: crystal structure database for inorganic compounds. Release 2014/15. ASM International, Materials Park

21. Robinel E, Carette B, Ribes M (1983) Silver sulfide based glasses (I): glass forming regions, structure and ionic conduction of glasses in GeS_2–Ag_2S and GeS_2–Ag_2S–AgI systems. J Non-Cryst Solids 57:49–58

22. Moroz MV, Demchenko PYu, Mykolaychuk OG, Akselrud LG, Gladyshevskii RE (2013) Synthesis and electrical conductivity of crystalline and glassy alloys in the Ag_3GeS_3Br-GeS_2 system. Inorg Mater 49:867–871

23. Moroz M, Tesfaye F, Demchenko P, Prokhorenko M, Lindberg D, Reshetnyak O, Hupa L (2018) Determination of the thermodynamic properties of the $Ag_2CdSn_3S_8$ and Ag_2CdSnS_4 phases in the Ag–Cd–Sn–S system by the solid-state electrochemical cell method. J Chem Thermodyn 118:255–262

24. Moroz MV, Demchenko PYu, Prokhorenko SV, Moroz VM (2013) Physical properties of glasses in the Ag_2GeS_3-AgBr system. Phys Solid State 55:1613–1618

25. Moroz MV, Prokhorenko MV, Prokhorenko SV (2015) Determination of thermodynamic properties of Ag_3SBr superionic phase using EMF technique. Russ J Electrochem 51:886–889

26. Tesfaye F, Taskinen P (2014) Electrochemical study of the thermodynamic properties of matildite (β-$AgBiS_2$) in different temperature and compositional ranges. J Solid State Electrochem 18:1683–1694

27. Moroz MV, Prokhorenko MV, Rudyk BP (2014) Thermodynamic properties of phases of the Ag-Ge-Te system. Russ J Electrochem 50:1177–1181

28. Moroz MV, Prokhorenko MV (2014) Thermodynamic properties of the intermediate phases of the Ag-Sb-Se system. Russ J Phys Chem A 88:742–746

29. Moroz MV, Prokhorenko MV, Reshetnyak OV, Demchenko PYu (2017) Electrochemical determination of thermodynamic properties of saturated solid solutions of Hg_2GeSe_3, Hg_2GeSe_4, $Ag_2Hg_3GeSe_6$, and $Ag_{1.4}Hg_{1.3}GeSe_6$ compounds in the Ag–Hg–Ge–Se system. J Solid State Electrochem 21:833–837

30. Babanly M, Yusibov Y, Babanly N (2011) The EMF method with solid-state electrolyte in the thermodynamic investigation of ternary copper and silver chalcogenides. In: S Kara (Ed), InTech 57–78

31. Moroz MV, Demchenko PYu, Prokhorenko MV, Reshetnyak OV (2017) Thermodynamic properties of saturated solid solutions of the phases Ag_2PbGeS_4, $Ag_{0.5}Pb_{1.75}GeS_4$ and $Ag_{6.72}Pb_{0.16}Ge_{0.84}S_{5.20}$ of the Ag-Pb-Ge-S system determined by EMF method. J Phase Equilib Diffus 38:426–433

32. Voronin MV, Osadchii EG, Brichkina EA (2017) Thermochemical properties of silver tellurides including empressite (AgTe) and phase diagrams for Ag–Te and Ag–Te–O. Phys Chem Miner 44:639–653

33. Moroz MV, Prokhorenko MV (2015) Measurement of the thermodynamic properties of saturated solid solutions of compounds in the Ag-Sn-Se system by the EMF method. Russ J Phys Chem A 89:1325–1329

34. Moroz MV, Prokhorenko MV (2015) Determination of thermodynamic properties of saturated solid solutions of the Ag–Ge–Se system using EMF technique. Russ J Electrochem 51:697–702

35. Alverdiev IDzh, Bagkheri SM, Imamalieva SZ, Yusibov YuA, Babanly MB (2017) Thermodynamic study of Ag_8GeSe_6 by EMF with an Ag_4RbI_5 solid electrolyte. Russ J Electrochem 53:551–554

36. Yusibov YuA, Alverdiev IDzh, Ibragimova FS, Mamedov AN, Tagiev DB, Babanly MB (2017) Study and 3D modeling of the phase diagram of the Ag–Ge–Se system. Russ J Inorg Chem 62:1223–1233

37. Yusibov YuA, Alverdiev IDzh, Mashadieva LF, Babanly DM, Mamedov AN, Babanly MB (2018) Experimental study and 3D modeling of the phase diagram of the Ag–Sn–Se system. Russ J Inorg Chem 63:1622–1635

38. Voronin MV, Osadchii EG (2013) Thermodynamic properties of silver and bismuth sulfosalt minerals, pavonite ($AgBi_3S_5$) and matildite ($AgBiS_2$) and implications for ore deposits. Econ. Geol. 108:1203–1210

39. Barin I (1995) Thermochemical data of pure substance. VCH, Weinheim

40. Olin Å, Nolang B, Ohman L-O, Osadchii EG, Rosen E (2005) Chemical thermodynamics of Selenium. Elsevier, Amsterdam